Primljen / Received: 5.6.2024.
Ispravljen / Corrected: 22.7.2024.
Prihvaćen / Accepted: 7.9.2024.
Dostupno online / Available online: 10.12.2024.

Reliability and mechanical performance of timber–concrete composite beams in the non-linear domain

Authors:

Nabil Daanoune, MCE
University of Abderrahmane Mira Bejaia, Algeria
Faculty of Technology, Department of Civil Engineering
Laboratory of Construction Engineering and Architecture (LGCA)
nabil.daanoune@univ-bejaia.dz

Assoc.Prof. **Nassim Kernou**, PhD. CE
University of Abderrahmane Mira Bejaia, Algeria
Faculty of Technology, Department of Civil Engineering
Laboratory of Construction Engineering and Architecture (LGCA)
nassim.kernou@univ-bejaia.dz
Corresponding author

Prof. **Mamoun Fellah**, PhD. CE Mech.
Abbes Laghrour University, Algeria
Department of Mechanical Engineering
mamoune.fellah@univ-khenchela.dz

Prof. **Gamal A. El-Hiti**, PhD. MSc.
King Saud University, Saudi Arabia
Faculty of Applied Medical Sciences
Department of Optometry
gelhiti@ksu.edu.sa

Research Paper

Nabil Daanoune, Nassim Kernou, Mamoun Fellah, Gamal A. El-Hiti

Reliability and mechanical performance of timber–concrete composite beams in the non-linear domain

Different non-linear methods for calculating the reliability and mechanical performance of timber–concrete composite beams connected using threaded steel rods are compared. Two distinct approaches are used and validated using experimental data: a three-dimensional finite-element model developed using ABAQUS and an analytical study using a frozen shear method. The structural reliabilities of the beams were assessed using the MCS, FORM, and SORM methods, in which the geometric and mechanical input characteristics were treated as random variables. Certain parameters significantly affect beam failure, such as the timber's bending resistance, the concrete's compressive resistance, and the degree of composite action.

Key words:
non-linear modelling, finite element, reliability, performance, timber concrete composite beam, probability of failure

Prethodno priopćenje

Nabil Daanoune, Nassim Kernou, Mamoun Fellah, Gamal A. El-Hiti

Pouzdanost i mehanička svojstva spregnutih nosača drvo-beton u nelinearnome području ponašanja

U radu se uspoređuju se različite nelinearne metode za proračun pouzdanosti i mehaničkih svojstava spregnutih nosača drvo-beton povezanih čeličnim navojnim šipkama. Primijenjena su dva različita pristupa koja su provjerena uporabom eksperimentalnih podataka: trodimenzionalni model konačnih elemenata razvijen uporabom računalnog programa ABAQUS i analitičko ispitivanje primjenom metode smrznutog posmika. Pouzdanost nosača procijenjena je primjenom metoda MCS, FORM i SORM, u kojima se geometrijski i mehanički ulazni parametri opisuju kao slučajne varijable. Na otkazivanje nosača znatno utječu parametri kao što su otpornost drva na savijanje, otpornost betona na tlak i stupanj sprezanja.

Ključne riječi:
nelinearno modeliranje, konačni element, pouzdanost, ponašanje konstrukcije, spregnuti nosač drvo-beton, vjerojatnost otkazivanja

1. Introduction

Recently, mixed timber–concrete structures have gained traction as a promising construction technology [1]. This technology has significant potential for application in the building industry, particularly in the construction of multi-story high-rise timber structures [2, 3]. Their structural performance, both in the short and long term, is highly promising.

Extensive research has been conducted over the last 30 years to investigate the performance of these structures, including various small- and large-scale tests and analytical studies [4, 5]. The reliability of timber–concrete composite structures, expressed in terms of the reliability index or failure probability, is a fascinating factor for studying their performance and mechanical behaviour [6, 7]. With the recent practice of reliability-based design of timber structures, analysing their reliability has become increasingly important [8-10].

A few studies have linked the reliability index to the reliability design philosophy. Bulleit [11] developed an approximate reliability model for timber systems in which the ultimate capacity was estimated from the failure of the constituent elements. Kirkegaard et al. [12] assessed timber structures with an emphasis on strength owing to the ductility of the connection. Kohler and Svensson [13] developed a calibration approach that considers uncertainty in the damage accumulation model. Jockwer et al. [14] evaluated the failure behaviour and reliability of timber connections with multiple dowel-type fasteners. Li et al. [15] adjusted the load duration factor for the Chinese standard based on a reliability approach in which the impact of the load ratios and wood strength variation coefficients on the load duration factor was established.

The non-linear behaviour of timber–concrete composite beams is complex. Therefore, reliability studies have been conducted to better understand the mechanical behaviour and failure mechanism of the constituent elements and their reliability [16-18]. Several limit state functions can express the failure of a composite beam either at the ultimate limit state for the strength capacity limit or in the serviceability limit state for excessive deformations. Three ultimate limit state functions were proposed to express the failure of the beam based on the gamma and frozen shear methods [19-21]. The first limit state function expresses the failure at the connectors, the second one characterizes the failure by compression of the concrete, and the last one is the failure by bending of the timber. The sensitivity of the random variables to the structural safety of the composite beam was evaluated from the results obtained using the FORM method of the three limit state functions, providing originality for this study [22, 23].

This paper focuses on the failure mechanisms of the elements constituting timber–concrete composite beams; however, the proposed approach can also be applied to the reliability evaluation and updating of steel–concrete structures subjected to other deterioration processes. This paper addresses the sensitivity of random variables to the structural safety of a composite beam based on the proposed mechano-reliability coupling. In addition, the effects of the input parameters on the non-linear behaviour of the composite beam are investigated to understand the non-linear behaviour of the beam based on the reliability model and the three proposed limit-state functions.

2. Materials and methods

2.1. Eurocode 5 and the gamma method

The gamma method, presented in Eurocode 5, part 1-1 (CEN, 2004) [20], concerns composite beams of various materials. It applies to timber–concrete composite systems within the elastic range. The following assumptions are made: The slab has only one load-bearing direction and is supported by simple supports on the span beam L. A connection system with rigidity K_s links the wood and concrete components in the mixed structure. The spacing between the connectors varies uniformly based on the shearing force or was maintained constant. The application of a load in the transverse direction creates internal forces along the longitudinal axis of the beam. Materials such as timber and concrete exhibit elastic linear behaviour. Planar sections remain in each element but not in the overall system. The composite sections opposite 1 and 2 represent concrete and timber, respectively.

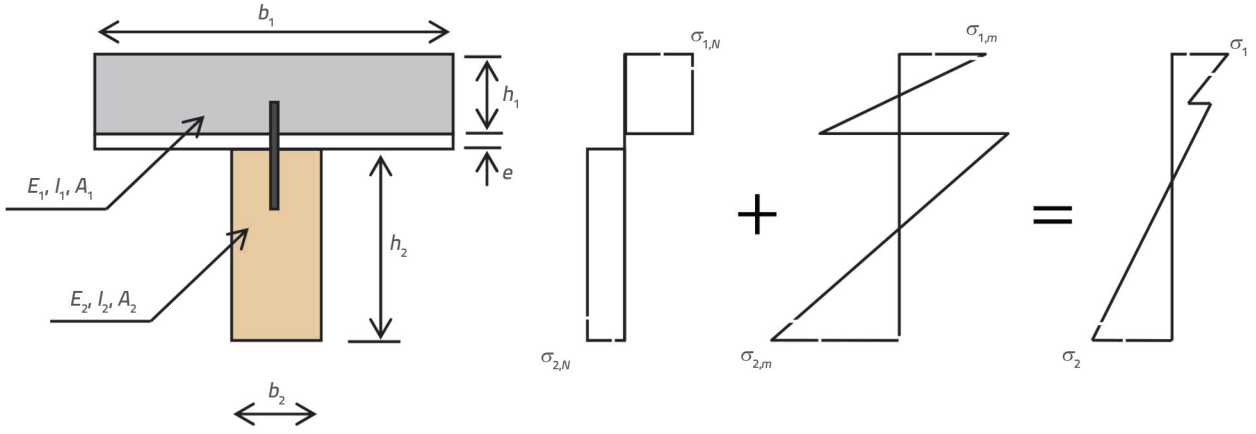

Figure 1. Composite section and stress distribution (E_1 - longitudinal modulus of elasticity of concrete, I_1 - inertia of concrete section, A_1 - section of concrete, E_2 - longitudinal modulus of elasticity of wood, I_2 - inertia of the section of wood, A_2 - section of wood, and e: thickness of the lost formwork

This method uses the effective bending stiffness (EI_{eff}) and load–deflection behaviour to calculate the slip modulus (k_s) and yield strength (Qy) of the connection. The shear coefficient (γ) is introduced to reduce the effective bending stiffness and is defined as follows:

$$\gamma = \frac{1}{1+\frac{\pi^2 \cdot E_1 \cdot A_1}{k_s \cdot L^2}} \quad (1)$$

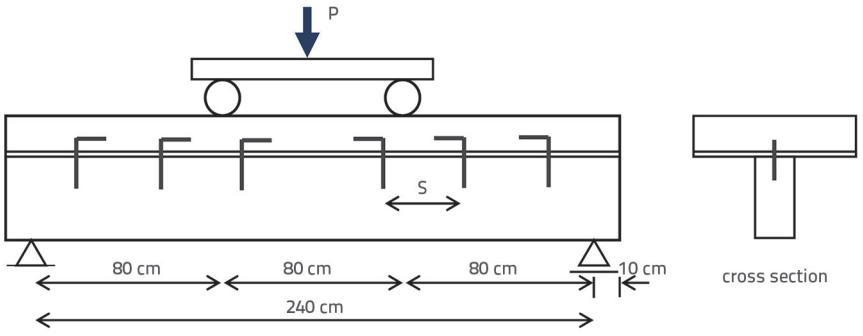

Figure 2. Layout of the four-point bending test

The value of k_s is obtained by dividing K_s by s. The coefficient γ = 0 applies to the nil composite action, whereas γ = 1 indicates the total composite action. The stiffness-effective bending (EI_{eff}) and internal lever arms (a_1 and a_2) can be calculated.

$$EI_{eff} = E_1(I_1+\gamma A_1 a_1^2) + E_2(I_2+A_2 a_2^2) \quad (2)$$

$$a_2 = \frac{\gamma E_1 A_1 (h_1 + h_2 + 2e)}{2(\gamma E_1 A_1 + E_2 A_2)} \quad (3)$$

$$a_1 = \frac{h_1 + h_2 + 2e}{2} - a_2 \quad (4)$$

The deflection of a single-span beam under a concentrated load (F=P/2) is located at L/3 from the ends of the beam, and the internal stresses of the system are calculated using the effective bending stiffness.

$$f = \frac{23PL^3}{1296 \cdot EI_{eff}} \quad (5)$$

$$\sigma_1 = \sigma_{1,N} \pm \sigma_{1,m} = \frac{\gamma E_1 a_1 M}{EI_{eff}} \pm \frac{E_1 h_1 M}{2EI_{eff}} \quad (6)$$

$$\sigma_2 = \sigma_{2,N} \pm \sigma_{2,m} = \frac{\gamma E_2 a_2 M}{EI_{eff}} \pm \frac{E_2 h_2 M}{2EI_{eff}} \quad (7)$$

The formulas are in Appendix B of Eurocode 5 [20].

2.2. Frozen shear method

Entirely linear models cannot adequately represent the behaviour of composite systems because the plasticity of the connectors affects the results at high loads. The fixed shear method proposed by van der Linder [24] is derived from the gamma method and assumes that the shear forces in each connector are frozen when they reach their yield point (Q_y). These forces act plastically at their respective loading level [21]. When the connectors yield, the timber and concrete sections can slip relative to each other, resulting in a lack of composite action and a reduction in the effective bending stiffness at EI_{min} [24]. This method considers the same basic assumptions as the gamma method, except for the elastic–plastic load–slip relationship of the connection [21]. The force in the connector can be determined using Eq. (8).

$$q = \frac{\gamma E_1 A_1 a_1 V}{EI_{eff}} \le Q_y \quad (8)$$

Where V is the maximum shear force.
When the connectors reach the plasticity domain, all terms representing the bending stiffness (EI_{eff}) are replaced by EI_{min}. This value corresponds to the bending stiffness of the composite section with a nil composite action.

$$EI_{min} = E_1 I_1 + E_2 I_2 \quad (9)$$

2.3. Data of the beam tested

The selected beam was a timber–concrete composite beam connected by an HA12 steel rod tested in bending at four points until failure [25]. The properties of the concrete part of the beam are shown in Table 1, the wooden part in Table 2, and the properties of the fasteners in Table 3.

Table 1. Concrete section properties

Settings	Average	Standard deviation	Reference
b_1	500 [mm]	-	[25]
h_1	50 [mm]	-	[25]
E_1	28800 [MPa]	10 %	[25]
f_c^{o}: compressive strength	25.1 [MPa]	11 %	[25]

Table 2. Timber section properties

Settings	Mean value	Standard deviation	Reference
b_2	65 [mm]	-	[25]
h_2	160 [mm]	-	[25]
e	10 [mm]	-	[25]
E_2	12200 [MPa]	12 %	[25]
f_{co}: concrete compressive strength	43.8 [MPa]	5 %	[25]
f^{mo}: timber bending strength	81.5 [MPa]	9 %	[25]

Table 3. Connection properties

Settings	Mean value	Standard deviation	Reference
K_s: sliding stiffness	2920 [N/mm]	3 %	[25]
F_y: ultimate shear strength		19 %	[25]
Ø: rod diameter	12 [mm]	-	[25]
S: spacing	100 [mm]	-	[25]

2.4. Finite element modelling

2.4.1. Modelling of materials

Concrete

The concrete used in this study was ordinary concrete with different tension and compression behaviours. For this, we selected SARGIN's law for the behaviour of concrete in compression [26] and the GRELAT model for the behaviour of concrete in traction [27]. The non-linear elastic behaviour in compression shown in Figure 3.a is expressed by the following SARGIN law:

$$\sigma = f_{cj} \cdot \frac{k_b \cdot \bar{\varepsilon} + (k_b' - 1) \cdot \bar{\varepsilon}^2}{1 + (k_b - 2) \cdot \bar{\varepsilon} + k_b' \cdot \bar{\varepsilon}^2} \quad (10)$$

Where $\bar{\varepsilon} = \varepsilon/\varepsilon_{b0}$, $k_b = (E_{b0}\varepsilon_{b0})/f_{cj}$ and E_{b0} is the modulus of elasticity of the concrete.

Value $k'_b = k_b - 1$ was set up based on [28], for concrete $f_{cj} \leq 30$ MPa.

The tensile behaviour of concrete is shown in Figure 3.b for cracking with the participation of tense concrete expressed by the GRELAT model [27]:

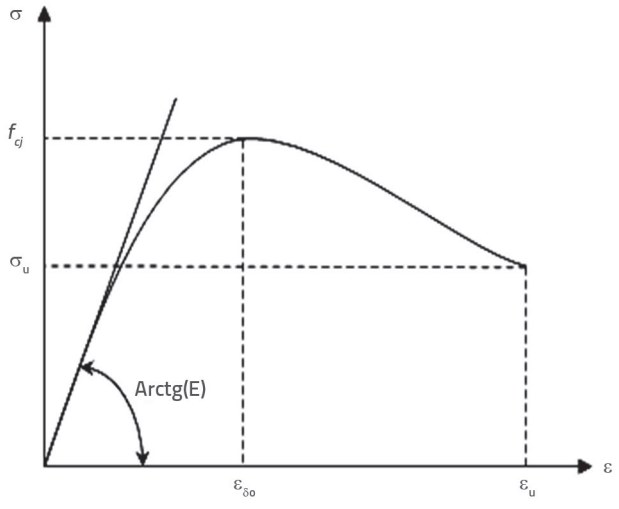

Figure 3a. Behaviour of ordinary concrete in compression

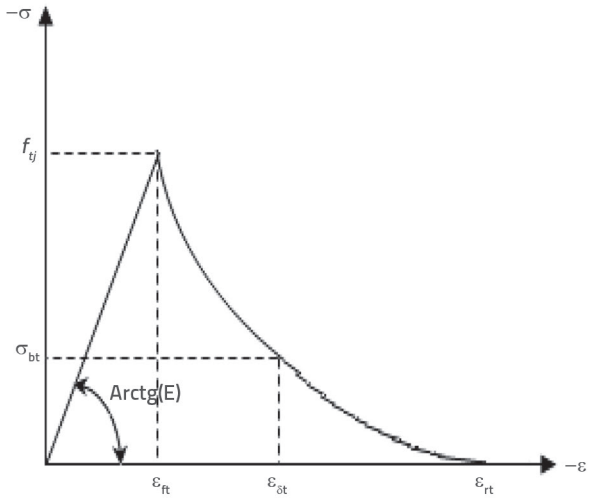

Figure 3b. Behaviour of ordinary concrete in tension

$$\sigma_{bt} = -f_{tj} \cdot \frac{(\varepsilon_{bt} - \varepsilon_{rt})^2}{(\varepsilon_{rt} - \varepsilon_{ft})^2} \quad (11)$$

Where f_{tj} is the tensile strength of concrete, ε_{ft} is the tensile strain corresponding to f_{tj}, ε_{rt} is the deformation corresponding to the plastification of the most tense steel, and ε_{bt} is the deformation of the most tense concrete fibre.

Steel

The steel materials used in our study were reinforcement steel HA 10 for the reinforcement of the concrete slab and HA12 for the timber–concrete connection. This steel exhibits elastoplastic and symmetrical behaviours under tension and compression, as shown in Figure 4, according to [20].

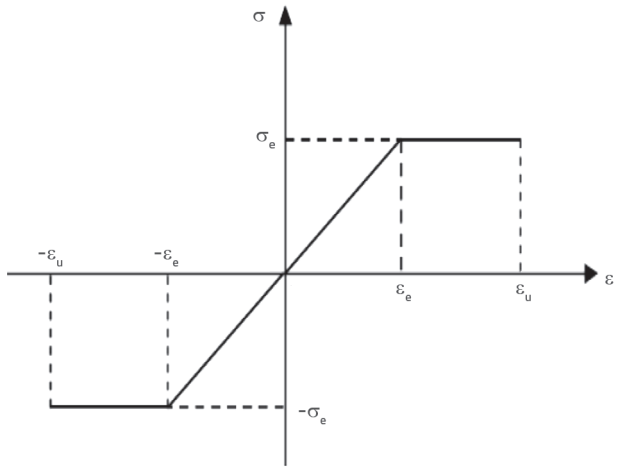

Figure 4. Stress–strain relationship for reinforcing bars and steel connections, where ε_e is the elastic limit strain of the steel, ε_e is the yield stress of the steel, and ε_u is the ultimate strain of the steel

Timber

Solid timber is considered to be an anisotropic material because of the variations in its physical and mechanical properties depending on its direction. It is classified in Eurocode 5 according to its mechanical properties. It can be replaced by other timbers with similar mechanical properties, such as Iroko wood or Mahogany African [29], which are available in the same region of West Africa. Mahogany African is classified in Eurocode 5 as a solid timber hardwood from D50 to D70 [20], according to the maximum mechanical resistance classes reached for the main types of timber used in construction.

Timber is also modelled as an orthotropic material according to [30, 31], and its behaviour varies in three perpendicular directions: longitudinal (parallel to the fibre), radial, and transverse. Timber is elastoplastic under compression [20] and elastic under traction. ABAQUS explicitly applies Hill's constraint function [32] to allow anisotropic behaviour Eq. (12).

$$f(\sigma)=\sqrt{F\left(\sigma_y-\sigma_z\right)^2+G\left(\sigma_z-\sigma_x\right)^2+H\left(\sigma_x-\sigma_y\right)^2+2L\tau_{yz}^{\ 2}+2M\tau_{zx}^{\ 2}+2N\tau_{xy}^{\ 2}} \quad (12)$$

Or:

$$F=\frac{1}{2}\left(\frac{1}{R_{22}^{\ 2}}+\frac{1}{R_{33}^{\ 2}}-\frac{1}{R_{11}^{\ 2}}\right) \quad (13)$$

$$G=\frac{1}{2}\left(\frac{1}{R_{33}^{\ 2}}+\frac{1}{R_{11}^{\ 2}}-\frac{1}{R_{22}^{\ 2}}\right) \quad (14)$$

$$H=\frac{1}{2}\left(\frac{1}{R_{11}^{\ 2}}+\frac{1}{R_{22}^{\ 2}}-\frac{1}{R_{33}^{\ 2}}\right) \quad (15)$$

$$L=\frac{3}{2R_{23}^{\ 2}} \quad (16)$$

$$M=\frac{3}{2R_{13}^{\ 2}} \quad (17)$$

$$N=\frac{3}{2R_{12}^{\ 2}} \quad (18)$$

2.4.2. Mesh and interaction ABAQUS model

The ABAQUS/Explicit module was used to establish the 3D finite-element (FE) model. The C3D8R element was used to define the wooden beam mesh and concrete slab. The T3D2 element was used to define the reinforcing steel of the concrete slab and connectors. An embedded region constraint ensured the interaction between the reinforcement steel and concrete, thus facilitating the interaction of the connectors, wood, and concrete.

Tabe 4. Strength and stiffness properties of timber

Settings		Values	References
Modulus of elasticity in three directions: longitudinal (L), radial (R) and transverse (T)	E_L [MPa]	12200	[25]
	E_R [MPa]	1354	[29]
	E_T [MPa]	610	
Poisson's ratios (LR, LT, RT)	υ_{LR}	0.297	[29]
	υ_{LT}	0.641	
	υ_{RT}	0.604	
Modulus of elasticity in the directions (LR, LT, RT)	G_{LR} [MPa]	1074	[29]
	G_{LT} [MPa]	720	
	G_{RT} [MPa]	256	
Compression strength parallel to grain $f_{c,0}$ [MPa]		43.7	[25]
Tension strength parallel to the grain $f_{t,0}$ [MPa]		78	[30]
Compression strength perpendicular to the grain $f_{c,90}$ [MPa]		5	[30-29]
Shear strength f_v [MPa]		8.75	[30-29]
Anisotropic yield strength ratios	R11(+)	1	[30]
	R11(-)	0.56	
	R22 = R33	0.064	
	R12 = R13 = R23	0.194	

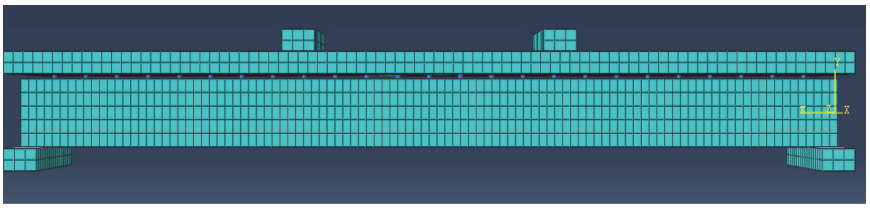

Figure 5. 3D ABAQUS model and meshing of the composite beam

2.5. Mechanical-reliability coupling

2.5.1. Reliability calculation methods

Three different methods were used: the Monte Carlo method, FORM, and SORM. Monte Carlo simulations are generally practical and represent real phenomena during sample tests. The principle of this method involves generating many simulations on the order of 10^n to calculate the failure probability [33] using the following law:

$$P_f = \frac{N_f}{N} \tag{19}$$

where N_f is the number of times the system fails, and N is the total number of simulations. Our study used a MATLAB command to generate N simulations with a given mean and standard deviation.

FORM method: This method is a first-order approximation of the Taylor series of the limit state function G(x) around point P*, called the design point. The method involves determining the reliability index (β), which is the closest distance between the origin (O) and point P* in centred standard space, reducing β, then providing access to an approximate failure probability P_f [33]. The reliability index was calculated using the Hasofer–Lind––Rackwitz–Fiessler algorithm Eq. (20).

$$\beta = \min_{g(u)=0} \sqrt{\sum_{i=1}^{n} u_i^2} \tag{20}$$

$$P_{f,\,FORM} = \Phi(-\beta) \tag{21}$$

Where Φ is the cumulative distribution function (CDF) (see Appendix 1)) [33].

SORM method: This method is a second-order approximation of the Taylor series of the limit state function G(x), based on the correction of the value of the failure probability obtained using FORM. For this method, we used the Breitung formula to calculate P_f [34].

$$P_{f,\,SORM} \approx \Phi(-\beta) \prod_{j=1}^{n-1} (1+\beta k_j)^{-1/2} \tag{22}$$

The principal curvatures (kj) are defined as the eigenvalues of matrix A such that its elements (aij) are defined as follows:

$$a_{ij} = \frac{(RDR')_{ij}}{\left|\nabla G(U^*)\right|} \; i, j = 1, 2, 3, \ldots, n-1 \tag{23}$$

Alternatively, D is the n x n Hessian matrix of the limit state function in the reduced centred normal space evaluated at the design point. R is the rotation matrix obtained using the Gram–Schmidt transformation (see Appendix 6) [34].

2.5.2. Connector failure

The force F_{r1} that causes the yielding of the connector was estimated using Eq. (8); we obtained $F_{r1} = (2EI_{eff}O_y)/(\gamma E_1 A_1 a_1) \approx 43{,}6$ kN.

2.5.3. Compressive failure of concrete

Estimating the force F_{r2}, which causes the rupture in compression of the concrete, in the limit state, we obtained $F_{r2} = (6EI_{eff}f_c)/(E_1 L(\gamma a_1 + 0{,}5h_1)) \approx 49$ kN.

2.5.4. Failure in wood bending

The force F_{r3}, which causes the rupture in the bending of the wood, was estimated as $F_{r3} = (12EI_{min}f_m)/(E_2 h_2 L) \approx 88$ kN.

2.5.5. Calculation of the probability of failure

The general form of the limit state function is G = R - S, where R is the resistance of the structure, and S is the imposed load. Three limit state functions were selected based on the following three failure modes:

$$G_1 = Q_y - \frac{\gamma E_1 A_1 a_1 F}{2EI_{eff}} \tag{24}$$

$$G_2 = f_c - \frac{FLE_1}{6EI_{eff}(\gamma a_1 + 0.5h_1)} \tag{25}$$

$$G_3 = 12f_m(E_1 I_1 + E_2 I_2) - FLE_2 h_2 \tag{26}$$

The random variables of each function are shown in Table 5.

Table 5. Random variables

Limit state functions	G_1	G_2	G_3	Distribution
Random variables	EI_{eff}	EI_{eff}	f_m	Normal
	E_1	E_1	E_1	Normal
	γ	γ	E_2	Normal
	F_y	f_c	-	Normal

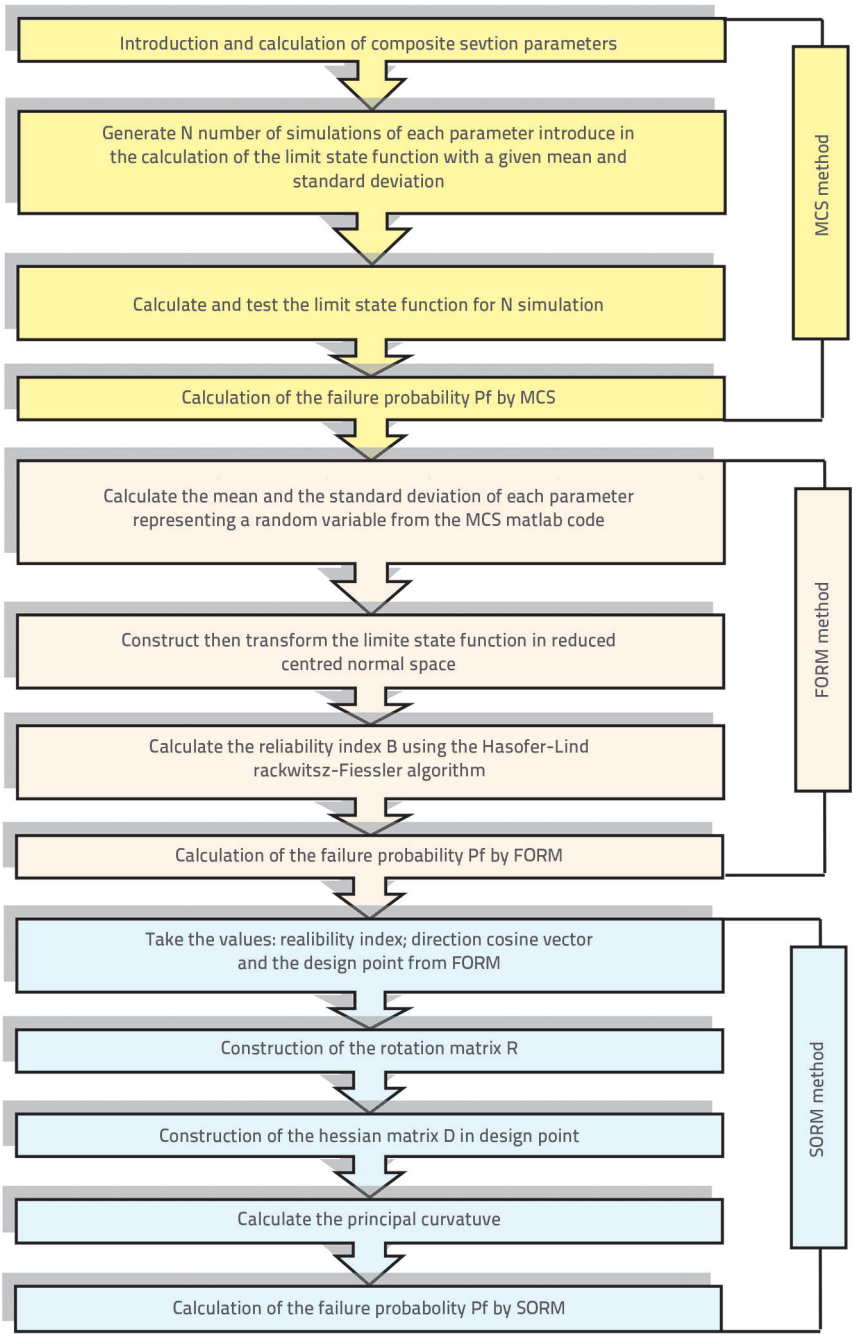

Figure 6. Mechano-reliability coupling flowchart and reliability methods used

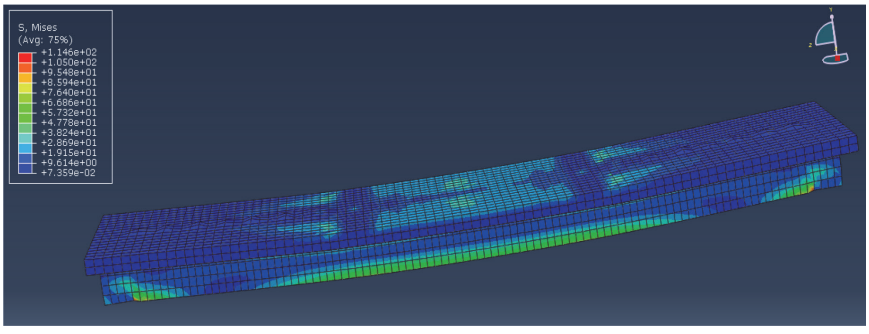

Figure 7. Stress distributions in timber beam and concrete slab at maximum load

The flowchart in Figure 6 shows the mechano-reliability coupling between the mechanical model and reliability methods used. Using the results obtained with the MATLAB script, we compared the failure probabilities of MCS, FORM, and SORM.

3. Results and discussion

3.1. ABAQUS results

Figure 7 shows the stress distributions in the timber beam and concrete slab. The stresses on the timber beam and concrete slab were under the maximum load. When the composite beam model reached the limit state, the upper fibres of the concrete exhibited the maximum stress, which ranged from 20 to 30 MPa. These stress values correspond to the compressive strength of concrete, which is 25.1 MPa. In the lower fibre of the timber beam, it reached 70 to 90 MPa, corresponding to the bending strength of timber, which is 81.5 MPa. The increase in the loading of the composite beam in the ABAQUS model showed the arrival at the limit stress of the concrete slab before the timber beam, which signalled the appearance of a crack at the upper fibre of the concrete slab before the final fracture by traction of the timber beam in the experiment [25].

Figure 8 shows the stress distribution in the connectors at the maximum load, which varied from 300 to 453 MPa at both ends of the crossbar and decreased to 0 at the connector installed in the middle of the timber beam. This indicated that the stress at the connectors exceeded the elastic limit of the connectors at 400 MPa.

Figure 9 compares load–deflexion curves at the mid-span for the two non-linear methods and the experimental data. The first part of the representation employed the frozen shear method, which is identical to the gamma method (Eurocode 5) [20]. Subsequently, the representation changed its slope in the second part at a load of 43 kN, which represented the beginning of the plasticity of the connectors, to avoid

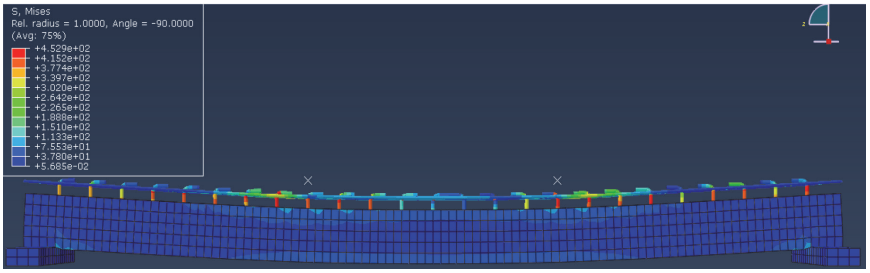

Figure 8. The stress distributions in the connection at the maximum load

considering the composite action in the composite beam. This representation exceeded the others in the FE method and experimental data because the non-linear behaviour in concrete, timber, and connectors was neglected.

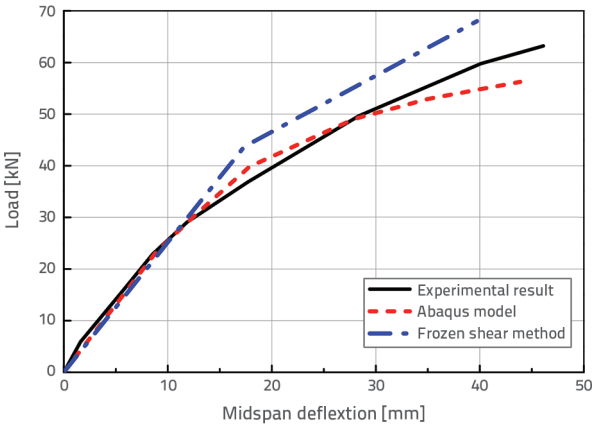

Figure 9. Load–deflexion curve of the timber–concrete composite beam

The results of the FE method closely matched those of the gamma method and experimentation until the end of the elastic part, reaching approximately 60 % of the maximum load, almost the same ratio observed by Du et al. [35] with some variations. This result was attributed to the simplicity of the elastoplastic behaviour law of timber and steel or the non-linear laws used in concrete.

Figure 10 compares the load–slip curves at the ends of the concrete slab and timber beam. A correspondence was observed between the results obtained using the FE method and the experimental data, which represented the actual behaviour of the composite beam.

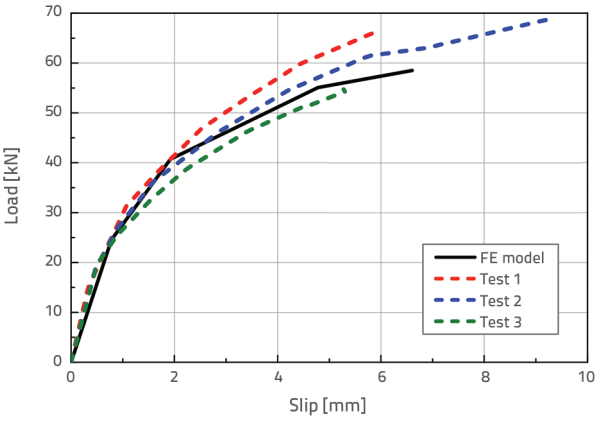

Figure 10. Load-slip curve of the timber–concrete composite beam

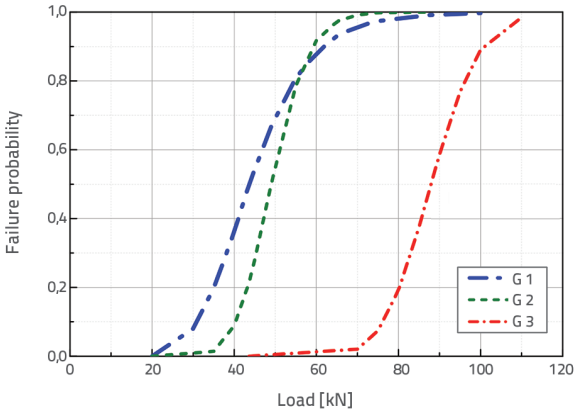

Figure 11. Variation in the failure probability of G1, G2, and G3 as a function of loading

Table 6. Failure probability for three limit state functions G_1, G_2 and G_3

Function	Failure probability P_f			
	Force applied	MCS	FORM	SORM
G_1	$F_{r1} \approx 43.6$ [kN]	0.4974	0.5104	0.5041
	$F_{r2} \approx 49$ [kN]	0.6676	0.6544	0.6547
	$F_{r3} \approx 88$ [kN]	1	0.9988	0.9999
G_2	F_{r1}	0.2165	0.2259	0.2239
	F_{r2}	0.5014	0.5030	0.5030
	F_{r3}	1	0.9999	1
G_3	F_{r1}	0	0	0
	F_{r2}	0		
	F_{r3}	0.5018	0.5082	0.5078

3.2. Reliability results

Table 6 lists the failure probability of each limit state function and the results obtained using the MATLAB, following all the steps indicated in the flowchart in Figure 6.

Figure 12 shows the variation in failure probability depending on the beam loading.

In the failure probability curves of the three functions in Figure 12, we observed that for the nonlinear limit state functions, SORM had a better approximation than the FORM because SORM approximates the limit state surface as a hyperboloid, whereas FORM approximates the surface as a tangential hyperplane. Therefore, SORM is more accurate. Most of the results obtained using SORM were close to those of MCS, as shown in Table 6. The MCS results were real and more exact than those of the iterative methods and those obtained by Yu et al. [36] and Morse et al. [37].

Therefore, the MCS results were the most rigorous of the three methods. Based on the results obtained from the failure, we noted the beginning of the plasticisation of the connector and a compression failure of the concrete before arriving at the bending failure of the timber. Subsequently, the composite beam lost a significant portion of its composite action when the connectors started yielding, resulting in a loss in beam solidarity. The timber beam and concrete slab resisted individually until their weaker parts failed.

3.3. Sensitivity analysis

A sensitivity analysis was used to assess the significance of the design variables employed in our research on the response of the composite beam. This survey identified the most critical variables for effective decision-making, primarily for numerous variables. The primary objective of this study was to identify the most influential variables.

The proposed method evaluated the impact of random variables on the safety of a structure. To achieve this, we aimed to determine the direction cosines of the most likely failure points in a standard probability space. The squares of these direction cosines are shown in Figures 12–14, highlighting the importance of these parameters in the limit state functions [22].

In our specific case, the sensitivity analysis explored the effect of the input parameters on the non-linear behaviour of the composite beam. Three values of F (concentrated force leading to rupture) were employed to compare and study the sensitivity variations based on the application level of F. The values of F applied to the composite beam were $Fr_1 \approx 43.6$ kN, $Fr_2 \approx 49$ kN, and $Fr_3 \approx 88$ kN. This analysis investigated the variation in sensitivity with applied load. The results are shown in Figures 12–14.

The most influential parameter on the first limit state function (G1) was the ultimate shear strength of the connector (Fy), with a value of 64 % with F1, decreased towards 60 % with F2, and decreased again towards 40 % with F3. This is because it is a resistance

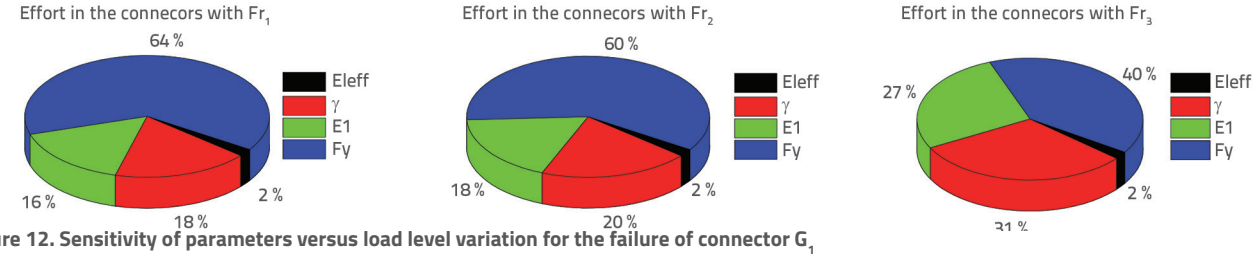

Figure 12. Sensitivity of parameters versus load level variation for the failure of connector G_1

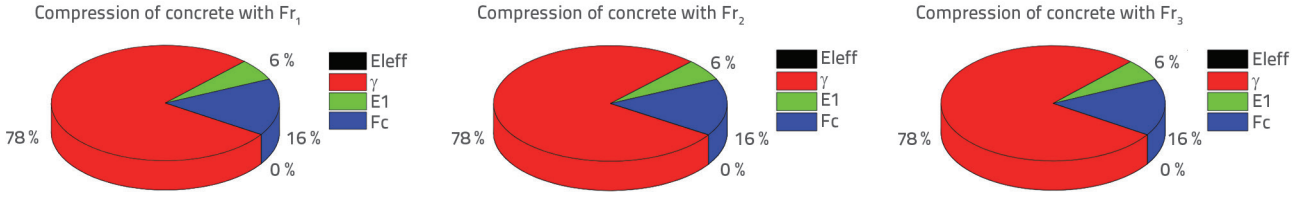

Figure 13. Sensitivity of parameters versus load level variation for concrete compressive failure G_2

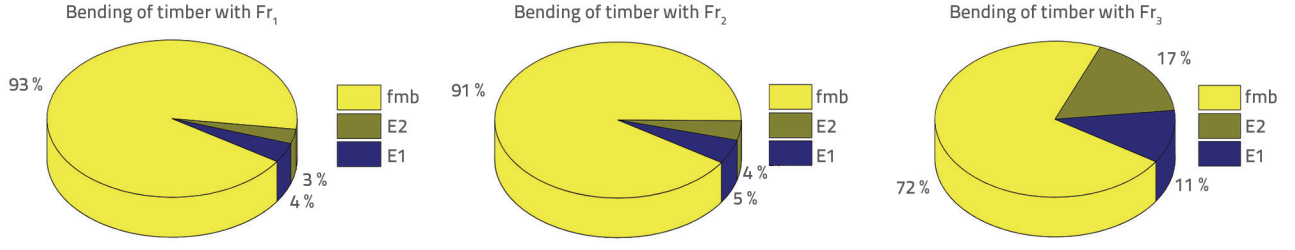

Figure 14. Sensitivity of parameters versus load level variation for concrete compressive failure G_3

parameter, unlike other parameters of loads E1 and which were 16 % and 18 %, respectively, with F1 and increased to 27 % and 31 %, respectively, with F3 (Figure 12). Thus, we can conclude that, to ensure the reliability of the connector, the ultimate shear strength of the connector Fy must be stronger. This parameter enables good interfacial shear resistance between the wood and concrete, resulting in a high degree of composite action.

For the second limit state function, G2 was the compressive strength of concrete (Fc), which was 57 % with F1, decreased towards 52 % with F2, and decreased to 16 % after the concrete had failed with F3. This is because it is a resistance parameter, unlike the other parameters E1 and γ, which were 38 % and 1 %, respectively, with F1 and changed to 6 % and 78 %, respectively, with F3 (Figure 13). Thus, we can conclude that, to ensure the reliability of the concrete slab, the compressive strength of the concrete F_c must be stronger.

After failure at the level of the connectors and concrete slab, the wooden beam was the only component of the resistant composite beam. The study of the sensitivity of the parameters in the limit state function G3 showed the effect of the bending resistance of wood (fm) on the safety margin of the limit state function G3, with a value of 93 % with F1 and decreasing to 72 % with F3. In contrast, the moduli of elasticity E1 and E2 varied by 4 % and 3 %, respectively, with F1, and changed to 11 % and 17 %, respectively, with F3 (Figure 14).

At the end of the sensitivity study, we could not directly validate the results of our study because of the difference in the limit state functions used by other researchers. However, we were able to compare the similarities and common factors found. In this study, we observed that the parameters that play a role in the resistance of a material of the structures studied have a significant influence on the reliability of our structure, such as the compressive resistance of concrete, bending resistance, and tensile strength of timber, which can be confirmed by Kernou et al. [37-39] and Lydia et al.[40].

4. Conclusion

A methodology for modelling and updating the reliability of timber–concrete composite beams was proposed. It considers failure scenarios for each component of the beam, and includes a numerical study to assess its reliability.

The effects of reliability assessment of the connector force, concrete compression, and timber bending were studied. The results showed the initial plastification, compressive concrete failure, and flexural failure of the timber because solid wood has a higher bending strength than wood glulam (f_m = 81.7 MPa).

The study observed that the shear resistance parameter (fy) has a significant role (64 %) in the reliability and failure of connector elements. The compressive strength of concrete parameter (f_c) also has a significant impact (52 %) on concrete failure, whereas the bending resistance parameter (f_m) has a 72 % impact on wood failure. These parameters should be considered when selecting the materials and dimensions of composite beams. The results showed that the probability of failure varies with the applied force. For F_r = 56 kN, the connectors and concrete have an 85 % probability of failure, whereas the wooden element has almost zero probability. The reliability of timber is most affected by flexural strength, whereas connectors and concrete are most affected by yield strength and compressive strength, respectively. The applied force significantly affects the behaviour of the composite beam. The reliability assessment method can be used as a decision-support tool to establish a maintenance and inspection plan for composite steel–concrete beams.

REFERENCES

[1] Belabid, A., Elminor, H., Akhzouz, H.: Hybrid construction technology, towards a mix that satisfies the requirements of the 21st century: state of the art and future prospects, Future Cities and Environment, 8 (2022) 1, pp. 1-16, https://doi.org/10.5334/fce.159

[2] Shi, B., Liu, W., Yang, H., Ling, X.: Long-term performance of timber-concrete composite systems with notch-screw connections, Engineering Structures, 213 (2020), p. 110585, https://doi.org/10.1016/j.engstruct.2020.110585

[3] Wong, S.W.: Calibrating wood products for load duration and rate: a statistical look at three damage models, Wood Science and Technology, 54 (2020) 6, pp. 1511-1528, https://doi.org/10.48550/arXiv.2002.03537.

[4] Ceccotti, A., Fragiacomo, M., Giordano, S.: Long-term and collapse tests on a timber-concrete composite beam with glued-in connection, Materials and structures, 40 (2007), pp. 15-25, https://doi.org/10.1617/s11527-006-9094-z.

[5] Dias, A.M.P.G., Van de Kuilen, J.W., Lopes, S., Cruz, H.: A non-linear 3D FEM model to simulate timber–concrete joints, Advances in Engineering Software, 38 (2007) 8-9, pp. 522-530, https://doi.org/10.1016/j.advengsoft.2006.08.024

[6] Cheng, F., Hu, Y.: Reliability analysis of timber structure design of poplar lumber with nondestructive testing methods, BioResources, 6 (2011) 3, pp. 3188-3198, https://bioresources.cnr.ncsu.edu/BioRes_06/BioRes_06_Unsecured/BioRes_06_3_3188_Cheng_Hu_Reliability_Anal_Timber_Nondestruc_1621.pdf

[7] Velimirovic, N.: Time-dependent reliability analysis of timber-concrete composite beams, Periodica Polytechnica Civil Engineering, 61 (2017) 4, pp. 718-726, https://doi.org/10.3311/PPci.10276

[8] Svensson, S., Thelandersson, S. Larsen, H.J.: Reliability of timber structures under long term loads, Materials and Structures, 32 (1999), pp. 755-760, https://doi.org/10.1007/BF02905072

[9] Drummond, I., Kermani, A., Wamuziri, S.C.: Reliability of timber structural systems: a review, Proceedings of the Institution of Civil Engineers-Structures and Buildings, 146 (2001) 1, pp. 101-108, https://doi.org/10.1680/stbu.2001.146.1.101

[10] Köhler, J.: Reliability of Timber Structures (No. 301). vdf Hochschulverlag AG, 2001, https://doi.org/10.3929/ethz-a-005454370

[11] Bulleit, W.M.: Reliability model for wood structural systems, Journal of Structural Engineering, 112 (1986) 5, pp. 1125-1132, https://doi.org/10.1061/(ASCE)0733-9445(1986)112:5(1125)

[12] Kirkegaard, P.H., Sørensen, J.D., Čizmar, D., Rajčić, V.: System reliability of timber structures with ductile behaviour, Engineering Structures, 33 (2011) 11, pp. 3093-3098, https://doi.org/10.1016/j.engstruct.2011.03.011

[13] Kohler, J., Svensson, S.: Probabilistic representation of duration of load effects in timber structures, Engineering Structures, 33 (2011) 2, pp. 462-467, https://doi.org/10.1016/j.engstruct.2010.11.002

[14] Jockwer, R., Fink, G., Köhler, J.: Assessment of the failure behaviour and reliability of timber connections with multiple dowel-type fasteners, Engineering Structures, 172 (2018), pp. 76-84, https://doi.org/10.1016/j.engstruct.2018.05.081.

[15] Li, Z., Zheng, X., Ni, C., Tao, D., He, M.: Reliability-based investigation into the duration of load effect for the design of timber structures based on Chinese standard, Structural Safety, 87 (2020), p. 102001, https://doi.org/10.1016/j.strusafe.2020.102001

[16] Cvetković, R., Ranković, S., Mišulić, T.K., Kukaras, D.: Experimental analysis of mechanical behavior of timber-concrete composite beams with different connecting systems, Buildings, 14 (2024), p. 79, https://doi.org/10.3390/buildings14010079

[17] Mirdad, M.A.H., Chui, Y.H., Tomlinson, D.: Capacity and failure-mode prediction of mass timber panel–concrete composite floor system with mechanical connectors, Journal of Structural Engineering, 147 (2021) 2, p. 04020338, https://doi.org/10.1061/(ASCE)ST.1943-541X.0002909

[18] Frangi, A., Fontana, M.: Elasto-plastic model for timber-concrete composite beams with ductile connection, Structural Engineering International, 13 (2003) 1, pp. 47-57, https://doi.org/10.2749/101686603777964856

[19] Borgström, E., Karlsson, R.: Design of timber structures-structural aspects of timber construction. Swedish Forest Industries Federation. Volume 1. Swedish Wood, 2016

[20] European Committee for Standardization (CEN). EN 1995-1-1: Eurocode 5: Design of timber structures-Part 1-1: General-Common rules and rules for buildings, 2004

[21] Zhang, C.: Analysis of the timber-concrete composite systems with ductile connection, University of Toronto (Canada), 2013

[22] Kernou, N., Bouafia, Y.: Development of new approach in reliability analysis for excellent predictive quality of the approximation using adaptive kriging, International Journal of Engineering Research in Africa, 44 (2019), pp. 44-63, https://doi.org/10.4028/www.scientific.net/JERA.44.44

[23] Zhou, C., Li, C., Zhang, H., Zhao, H., Zhou, C.: Reliability and sensitivity analysis of composite structures by an adaptive Kriging based approach, Composite Structures, 278 (2021), p. 114682, https://doi.org/10.1016/j.compstruct.2021.114682

[24] Van der Linden, M.L.: Timber-concrete composite beams, Heron, 44 (1999) 3, pp. 215-236

[25] Denouwé, D.D.: Étude des performances mécaniques des poutres et planchers mixtes bois-béton – Influence du mode de connexion (Doctoral dissertation, University of Paris), 2018, https://doi.org/10.13140/RG.2.2.36282.52161

[26] Youssef, M.A., Moftah, A.: General stress–strain relationship for concrete at elevated temperatures, Engineering Structures, 29 (2007) 10, pp. 2618-2634, https://doi.org/10.1016/j.engstruct.2007.01.002

[27] Iguetoulene, F., Bouafia, Y., Kachi, M.S.: Nonlinear modeling of three-dimensional reinforced and fiber concrete structures, Frontiers of Structural and Civil Engineering, 12 (2018), pp. 439–453. https://doi.org/10.1007/s11709-017-0433-7

[28] Ramos, L., Pereira, S., Penna, S.S.: Nonlinear analysis method of concrete structures under cyclic loading based on the generalized secant modulus, Revista Ibracon de Estruturas e Materiais, 15 (2022), e15406, https://doi.org/10.1590/S1983-41952022000400006

[29] Kretschmann, D.E.: Wood handbook: wood as an engineering material, General Technical Report FPL-GTR-190, US Department of Agriculture, Forest Service, Forest Products Laboratory, 2010

[30] Kawecki, B., Podgórski, J.: 3D ABAQUS simulation of bent softwood elements, Archives of Civil Engineering, 66 (2020) 3, pp. 323-337, https://doi.org/10.24425/ace.2020.134400

[31] Du, H., Yuan, S., Liu, P., Hu, X., Han, G.: Experimental and finite element study on bending performance of glulam-concrete composite beam reinforced with timber board, Materials, 15 (2022) 22, p. 7998, https://doi.org/10.3390/ma15227998

[32] Dassault Systèmes, D.S.: Abaqus analysis user's guide, Abaqus Documentation, Simulia Corp., Waltham, MA, Report, 2016

[33] Grandhi, R.V., Wang, L.: Structural Reliability Analysis and Optimization: Use of Approximations (No. E-11684), 1999

[34] Haldar, A., Mahadevan, S.: Probability, Reliability and Statistical Methods in Engineering Design, Wiley, 2000

[35] Du, H., Yuan, S., Liu, P., Hu, X., Han, G.: Experimental and finite element study on bending performance of glulam-concrete composite beam reinforced with timber board, Materials, 15 (2022) 22, p. 7998, Pogreška! Referenca hiperveze nije valjana.

[36] Yu, B., Ning, C.L., Li, B.: Probabilistic durability assessment of concrete structures in marine environments: Reliability and sensitivity analysis, China Ocean Engineering, 31 (2017) 1, pp. 63-73, https://doi.org/10.1007/s13344-017-0008-3

[37] Morse, L., Khodaei, Z.S., Aliabadi, M.H.: Multi-fidelity modeling-based structural reliability analysis with the boundary element method, Journal of Multiscale Modelling, 8 (2017) 03n04, p. 1740001, https://doi.org/10.1142/S1756973717400017

[38] Kernou, N., Bouafia, Y., Khalil, B.: Reliability and punching shear resistance of slabs in non-linear domain, Građevinar, 67 (2015) 11, pp. 1051-1062, https://doi.org/10.14256/JCE.1295.2015

[39] Nassim, K., Messaoudene, L., Bennacer, L.: Effects of column damage on the reliability of reinforced concrete portal frames, Građevinar, 75 (2023) 1, pp. 53-63, https://doi.org/10.14256/JCE.3588.2022

[40] Lydia, M., Nassim, K.: Reliability analysis and comparative study of ordinary concrete and high performance concrete filled with steel tube under axial compression, International Journal of Engineering Research in Africa, 61 (2022), pp. 245-261, https://doi.org/10.4028/p-9h1zq6.

[41] Maslak, E., Stojić, D., Drenić, D., Mešić, E., Cvetković, R.: Strengthening timber–concrete composite girders with prestressed reinforcement, Građevinar, 72 (2020) 11, pp. 1001-1010, https://doi.org/10.14256/JCE.2784.2019

[42] Dayyani, M., Mortezaei, A., Rouhanimanesh, M.S., Marnani, J.A.: Performance of reinforced engineered cementitious composite square columns, Građevinar, 75 (2023) 1, pp. 31-21, doi: 10.14256/JCE.3503.2022

[43] Stepinac, M., Rajčić, V., Barbalić, J.: Influence of long term load on timber–concrete composite systems, Građevinar, 67 (2015) 3, pp. 235-246, https://doi.org/10.14256/JCE.1170.2014

[44] Vellaichamy, P., Veerasamy, S., Mangottiri, V.: Shear bond characteristics of steel concrete composite deck slab, Građevinar, 74 (2022) 5, pp. 393-401, https://doi.org/10.14256/JCE.3273.202